

Fourier Spectral Simulations and Gegenbauer Reconstructions for Electromagnetic Waves in the Presence of a Metal Nanoparticle

M. S. Min* T. W. Lee† P. F. Fischer‡ S. K. Gray§

August 25, 2004

Abstract. We describe Fourier Pseudospectral time-domain simulations, carried out in order to study light interacting with a metallic nanoscale object. The difficulty of using Fourier methods to accurately predict the electromagnetic scattering in such dielectric configuration arises from the discontinuity in the dielectric function along the surface of the metallic object. Standard Fourier methods lead to oscillatory behavior in approximating solutions that are nonsmooth or that have steep gradients. By applying the Gegenbauer reconstruction technique as a postprocessing method to the Fourier pseudospectral solution, we successfully reduce the oscillations after postprocessing.

Keywords. Fourier pseudospectral method, Gegenbauer reconstruction, postprocessing

1 Introduction

Metallic nanostructures, such as metal nanoparticles and nanoholes in thin metal films, are of considerable interest because of the possibility of creating surface plasmon excitations when interacting with light [2], [21]. Surface plasmons are collective electronic excitations that effectively concentrate and confine light energy. The manipulation of surface plasmons could lead to novel nanoscale optoelectronic devices [4], [16], [17].

Numerical simulations play an important role as a cost-effective tool for prototyping designs of such devices before manufacture. Among computational methods, Fourier methods have been naturally considered for problems with periodic features, such as planar waveguides and photonic crystal structures for integrated photonic devices, and their computational implementations and their error estimates have been analyzed in the literature [7], [10], [23].

In this paper we show how Fourier methods can also be applied to solve electromagnetic wave-scattering problems in metallic nanostructures, which do not possess periodic features in their configurations. Our focus is on mathematical reconstruction techniques for Fourier pseudospectral simulation data, using Fourier–Padé and Gegenbauer approximations [15], [19], [22], [23].

As a first step, we study light interacting with a small metal cylinder in a vacuum. The cylinder can be viewed as a silver nanowire with a diameter of 50 nm.

Before presenting the mathematical formulas, we give a brief overview of the mechanism describing the physics of scattering and absorption by a single nanoparticle. An applied oscillating field (i.e., an incident electromagnetic wave) induces a dipole moment in metallic region. These dipoles oscillate at the frequency of the applied field. The incident waves are absorbed in the metallic region and converted into a surface plasmon. Plasmons are the electron density waves associated with longitudinal waves propagating in matter through the collective motion of large number of electrons; a surface plasmon is defined as a coupled, localized electromagnetic field charge density oscillation propagating along the metallic surface.

Electromagnetic fields associated with the plasmon can be found from Maxwell’s equations if the dielectric response of the medium is lumped into corresponding complex dielectric constants under some condition. The real part of the metal dielectric constant must be negative, and its absolute value should be greater

*Mathematics and Computer Science Division, Argonne National Laboratory Argonne, IL, USA (mmin@mcs.anl.gov).

†Chemistry Division, Argonne National Laboratory, Argonne, IL, USA (twlee@tcg.anl.gov).

‡Mathematics and Computer Science Division, Argonne National Laboratory Argonne, IL, USA (fischer@mcs.anl.gov).

§Chemistry Division, Argonne National Laboratory, Argonne, IL, USA (gray@tcg.anl.gov).

than that of the imaginary part. The imaginary part of the metal dielectric constant determines how fast the plasmons decay by dissipating their energy into heat, which one wishes to have small.

We consider a y -polarized incident light traveling in the forward x direction. The incident light leaks an electrical field intensity, called an evanescent wave, into the metallic region. The amplitude of this evanescent wave decreases exponentially with distance from the interface, decaying over a distance of about one light wavelength from the surface. It may penetrate the metal cylinder and excite electromagnetic surface plasmon waves propagating within the metal cylinder surface. This surface plasmon is polarized in the plane of the surface and generates the huge enhancement of the fields at the metallic surface.

At this scale, the field of the incoming and outgoing wave cannot be resolved because the fields close to the metal are so large. As a result of the abrupt sharp change in magnitude around the metal surface, Fourier methods generate oscillatory behavior, referred to as Gibbs oscillations; hence, computations at high resolution are limited. However, the finite Fourier data contains enough information about the original solution that one can reexpress the data as a Padé or Gegenbauer finite expansion and can thus reduce the oscillations. In both cases, the reconstructions require obtaining the coefficients for the reconstructed approximations in terms of the Fourier coefficients. Implementations with Fourier–Padé reconstructions in [23] have successfully reduced the oscillations for Fourier pseudospectral solutions of nonlinear partial differential equations such as Burgers’ and Boussinesq equations. The Gegenbauer reconstructions have been applied to medical projection data computed by Fourier methods [22]. Here we apply the Gegenbauer reconstruction in Fourier pseudospectral time-domain simulations [19] of Maxwell’s equations. The computational results show that the Gegenbauer reconstructions successfully reduce the noise in the Fourier pseudospectral simulations.

This paper is organized as follows. Section 2 gives the formulation of Maxwell’s equations and the auxiliary differential equation for the current term from the Drude model [4], [16], [26]. The numerical discretizations in space and time and the setup of parameters are presented. Section 3 introduces the Gegenbauer polynomials and the postprocessing technique (i.e., the Gegenbauer reconstruction procedure) in one dimension. Their convergence behaviors are demonstrated for a nonperiodic function and some discontinuous functions. Section 4 presents the implementation in two dimensions and the reconstructed results of the Fourier pseudospectral solutions from the nanoparticle scattering simulations. Section 5 discusses the remaining issues concerning parameter optimizations for the reconstructions and computational automation with an appropriate error estimate. Section 6 briefly summarizes our research.

2 Formulations

Let us consider Maxwell’s equations governing planewave propagation in unbounded media

$$\frac{\partial D}{\partial t} = \nabla \times H - J, \tag{1}$$

$$\frac{\partial B}{\partial t} = -\nabla \times E, \tag{2}$$

$$\nabla \cdot D = \rho, \tag{3}$$

$$\nabla \cdot B = 0, \tag{4}$$

where E is the electric field and B the magnetic induction. The electric displacement D and the magnetic field H are defined by

$$D = \epsilon_0 E + P, \tag{5}$$

$$H = \frac{1}{\mu_0} B - M, \tag{6}$$

where P is the electric polarization (i.e., average electric dipole moment per unit volume), M the magnetization (i.e., average magnetic dipole moment per unit volume), ϵ_0 the permittivity, and μ_0 the permeability of free space.

Equations (1)–(6) are supplemented with constitutive relations having the form

$$J = \sigma E, \quad (7)$$

$$B = \mu H, \quad (8)$$

$$P = \epsilon_0 \chi_e E, \quad (9)$$

$$M = \chi_m H, \quad (10)$$

where σ is the conductivity, μ the permeability, χ_e the electric susceptibility, and χ_m the magnetic susceptibility, which vary depending on the medium.

In free space, the current J , polarization P , and magnetization M vanish. In the region occupied with metal, the magnetization M vanishes. The basic linear connection in the constitutive equations (7)–(10) can be nonlocal. Thus, using the Fourier transforms of the field quantities, rather than the fields themselves, one can write equations (5)–(6) in terms of the Fourier transform as

$$D(\omega) = \epsilon(\omega)E(\omega) \quad \text{and} \quad B(\omega) = \mu(\omega)H(\omega). \quad (11)$$

The phenomenological coefficients μ and ϵ can be complex, implying differences in phase between the various time-harmonic fields. If the imaginary part of any of the phenomenological coefficients of a medium is nonzero, the amplitude of a planewave will decrease as it propagates through such a medium because of absorption of electromagnetic energy. For metal, μ is close to unit, and the dielectric constant ϵ is complex valued, with a positive imaginary part and a negative real part. As a result, time-domain simulations are difficult; in particular, the negative real part of the dielectric function causes numerical instability. To overcome this, we use an alternative form for the current density J instead of using equation (7).

2.1 Drude Model

We start by examining the governing equations for the current term. The planewave solutions to the Maxwell's equations have the forms

$$E = E_0 e^{i(k \cdot x - \omega t)} \quad \text{and} \quad H = H_0 e^{i(k \cdot x - \omega t)}, \quad (12)$$

where k is the wave vector and ω is the time frequency. Then the frequency-domain Maxwell equation relating to (1) can be written as

$$-i\omega\epsilon(\omega)E(\omega) = \nabla \times H(\omega). \quad (13)$$

One can reexpress $\epsilon(\omega) = \epsilon_0 \epsilon_p$ as

$$\epsilon(\omega) = \epsilon_0 [\epsilon_\infty + (\epsilon_p - \epsilon_\infty)], \quad (14)$$

where ϵ_∞ is the infinite frequency value for the dielectric constant and ϵ_p will be specified later. Identifying the current density as

$$J(\omega) = -i\epsilon_0(\epsilon_p - \epsilon_\infty)E(\omega), \quad (15)$$

we rewrite equation (13) as

$$J(\omega) - i\omega\epsilon_0\epsilon_p E(\omega) = \nabla \times H(\omega). \quad (16)$$

Inverse Fourier transforming (16) gives

$$J(t) + \epsilon_0\epsilon_\infty \frac{\partial E(t)}{\partial t} = \nabla \times H(t). \quad (17)$$

The following is the Drude model [4], [16], [26] for the optical properties of a free-electron metal:

$$\epsilon_p = \epsilon_\infty - \frac{\omega_p^2}{\omega^2 + i\Gamma_p}, \quad (18)$$

where Γ_p is the Drude damping coefficient and ω_p is the plasmon frequency. This leads to

$$\frac{\partial^2 J(t)}{\partial t^2} + \Gamma_p \frac{\partial J(t)}{\partial t} = \epsilon_0 \omega_p^2 \frac{\partial E(t)}{\partial t}. \quad (19)$$

Reducing the order of the ordinary differential equation, we have

$$\frac{\partial J(t)}{\partial t} + \Gamma_p J(t) = \epsilon_0 \omega_p^2 E(t). \quad (20)$$

Equipped with equation (20) for the current term, we define the governing time-domain equations as

$$\epsilon \frac{\partial E}{\partial t} = \nabla \times H - J, \quad (21)$$

$$\mu \frac{\partial H}{\partial t} = -\nabla \times E, \quad (22)$$

$$\frac{\partial J}{\partial t} = \alpha J + \beta E, \quad (23)$$

where the phenomenological parameters in free space are

$$\epsilon = \epsilon_0, \quad \mu = \mu_0, \quad \alpha = 0, \quad \text{and} \quad \beta = 0 \quad (24)$$

and in the metallic region are

$$\epsilon = \epsilon_0 \epsilon_\infty, \quad \mu = \mu_0, \quad \alpha = -\Gamma_p, \quad \text{and} \quad \beta = \epsilon_0 \omega_p^2. \quad (25)$$

The values for the coefficients ϵ_∞ , Γ_p , and ω_p will be assigned by experimental measurement [16].

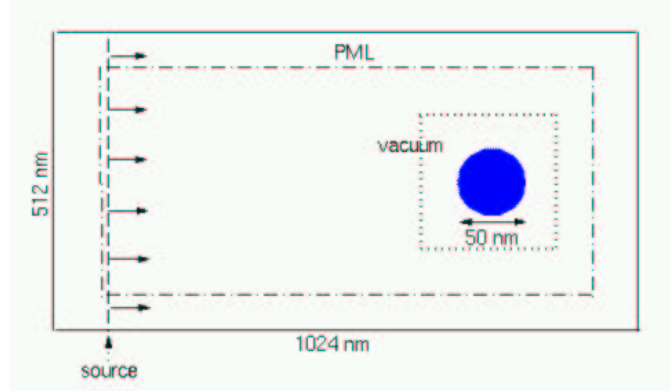


Figure 1: Computational domain

2.2 Numerical Scheme

The electromagnetic field vectors and the current vector are generally written by decomposing each component as follows:

$$E = (E_x, E_y, E_z), \quad H = (H_x, H_y, H_z), \quad \text{and} \quad J = (J_x, J_y, J_z). \quad (26)$$

Here we consider the transverse-electric mode in two dimensions:

$$E = (E_x, E_y, 0), \quad H = (0, 0, H_z), \quad \text{and} \quad J = (J_x, J_y, 0). \quad (27)$$

Let us define the computational domain on $[0, L_x] \times [0, L_y]$, where $L_x = 1024$ nm and $L_y = 512$ nm. The grid points are

$$x_i = \frac{L_x i}{N_x} (i = 0, \dots, N_x - 1), \quad (28)$$

$$y_j = \frac{L_y j}{N_y} (j = 0, \dots, N_y - 1). \quad (29)$$

Consider a metal cylinder with radius 25 nm whose center is placed at $x = 767.5$ nm and $y = 255.5$ nm in the computational domain (see Figure 1). The parameters of the equations in (25) for the metallic region are chosen as $\epsilon_\infty = 8.926$, $\Gamma_p = -3.08 \times 10^{14}$ Hz, and $\omega_p = 1.7577 \times 10^{16}$ Hz, as in [16], [17]. Since we simulate infinite-space solutions on a finite computational domain, we introduce an artificial absorbing layer in order to avoid the reflection from outgoing waves. The thickness of the absorbing layer is set to 28 nm and 40 nm in the x - and y -direction, respectively. We use the uniaxial perfectly matched layer (UPML) formulation [25], [26]; in this region the field intensity vanishes as it reaches to the boundary of the computational domain. Thus, it is reasonable to consider this problem as a periodic problem and to apply Fourier approximations globally in the computational domain.

Our numerical scheme is based on the Yee scheme [16], [27]. We simply replace the spatial derivative by the Fourier pseudospectral differentiation operator. At the time level $t^n = n\Delta t$, we have

$$\begin{aligned} \bar{E}_x^{n+\frac{1}{2}} &= \bar{E}_x^{n-\frac{1}{2}} + \frac{\Delta t}{\bar{\epsilon}} [D_y \bar{H}_z^n - \bar{J}_x^n], \\ \bar{E}_y^{n+\frac{1}{2}} &= \bar{E}_y^{n-\frac{1}{2}} + \frac{\Delta t}{\bar{\epsilon}} [D_x \bar{H}_z^n - \bar{J}_y^n], \\ \bar{H}_z^{n+1} &= \bar{H}_z^n + \frac{\Delta t}{\bar{\mu}_0} [D_x \bar{E}_y^{n+\frac{1}{2}} - D_y \bar{E}_x^{n+\frac{1}{2}}], \end{aligned} \quad (30)$$

and

$$\begin{aligned} \bar{J}_x^{n+1} &= \left[\frac{1 + \bar{\alpha}\Delta t/2}{1 - \bar{\alpha}\Delta t/2} \right] \bar{J}_x^n + \left[\frac{\bar{\beta}\Delta t}{1 - \bar{\alpha}\Delta t/2} \right] \bar{E}_x^{n+1/2}, \\ \bar{J}_y^{n+1} &= \left[\frac{1 + \bar{\alpha}\Delta t/2}{1 - \bar{\alpha}\Delta t/2} \right] \bar{J}_y^n + \left[\frac{\bar{\beta}\Delta t}{1 - \bar{\alpha}\Delta t/2} \right] \bar{E}_y^{n+1/2}, \end{aligned}$$

where the vector representations of the fields and parameters are defined, respectively, by

$$\bar{E}_x^n = [(E_x)_{00}, (E_x)_{10}, \dots, (E_x)_{ij}, \dots, (E_x)_{N_x-1, N_y-1}]^T \quad \text{for } (E_x)_{ij} = E_x(x_i, y_j), \quad (31)$$

$$\bar{\epsilon} = [\bar{\epsilon}_{00}, \bar{\epsilon}_{10}, \dots, \bar{\epsilon}_{ij}, \dots, \bar{\epsilon}_{N_x-1, N_y-1}]^T \quad \text{for } \bar{\epsilon}_{ij} = \epsilon(x_i, y_j). \quad (32)$$

2.2.1 Spatial Derivative

The Fourier pseudospectral differentiation operator in two dimensions can be represented by using a one-dimensional derivative operator. Let us consider a smoothly differentiable function $f(x)$ with period 2π , specified at N discrete grid points $x_0, \dots, x_i, \dots, x_{N-1}$, where $x_i = 2\pi i/N$. Fourier pseudospectral approximation of the function $f(x)$ is defined by

$$f_N(x) = \sum_{i=0}^{N-1} f(x_i) \Pi_i(x), \quad (33)$$

where $\Pi_i(x_j) = \delta_{ij}$ and $\Pi_i(x)$ is a Lagrange interpolation polynomial of degree N [12]. The polynomials $\Pi_i(x)$ are given explicitly by

$$\Pi_i(x) = \frac{1}{N} \sin[N(x - x_i)/2] \cot[(x - x_i)/2]. \quad (34)$$

In the pseudospectral method, the first derivatives $df_N(x)/dx$ at the grid points $x_{\hat{j}}$ are obtained in terms of the values $f(x_{\hat{i}})$ by simply differentiating (33):

$$\frac{df_N(x_{\hat{j}})}{dx} = \sum_{\hat{i}=0}^{N-1} f(x_{\hat{i}}) \frac{d\Pi_{\hat{i}}(x_{\hat{j}})}{dx} = (\hat{D}f)_{\hat{j}}, \quad (35)$$

where \hat{D} is a $N \times N$ matrix with elements

$$(\hat{D})_{\hat{j}\hat{i}} = \frac{d\Pi_{\hat{i}}(x_{\hat{j}})}{dx} = \begin{cases} 0 & (\hat{i} = \hat{j}) \\ \frac{(-1)^{\hat{i}+\hat{j}}}{2} \cot(x_{\hat{i}} - x_{\hat{j}}) & (\hat{i} \neq \hat{j}). \end{cases} \quad (36)$$

On the other hand, the trigonometric polynomial $\Pi_{\hat{i}}(x)$ of degree N has the equivalent representation [12] defined by

$$\Pi_{\hat{i}}(x) = \frac{1}{N} \sum_{k=-N/2}^{N/2-1} e^{ik(x-x_{\hat{i}})}. \quad (37)$$

Using (37), one can rewrite equation (33) as follows:

$$f_N(x) = \sum_{\hat{i}=0}^{N-1} f(x_{\hat{i}}) \frac{1}{N} \sum_{k=-N/2}^{N/2-1} e^{ik(x-x_{\hat{i}})} = \sum_{k=-N/2}^{N/2-1} \tilde{f}_k e^{ikx}, \quad (38)$$

defining

$$\tilde{f}_k = \frac{1}{N} \sum_{\hat{i}=0}^{N-1} f(x_{\hat{i}}) e^{-ikx_{\hat{i}}}, \quad (39)$$

which is in fact the discrete Fourier coefficient of $f(x)$. Thus one also can evaluate derivatives using equation (38) to obtain

$$\frac{df_N(x_{\hat{j}})}{dx} = \frac{1}{N} \sum_{k=-N/2}^{N/2-1} ik \tilde{f}_k e^{ikx_{\hat{j}}}. \quad (40)$$

Note that $f_N(x_{\hat{j}}) = f(x_{\hat{j}})$, $\hat{j} = 0, 1, \dots, N-1$, but their derivative $\frac{df_N}{dx}$ is not necessarily exact with $\frac{df}{dx}$ on the grids $x_{\hat{j}}$.

For the sake of convenience, here we use the physical space expression (35), rather than (40), for the spatial derivative D_x with respect to x in the scheme (30) using the one-dimensional derivative matrix $\hat{D}_x = [(\hat{D}_x)_{\hat{j}\hat{i}}]$ for $\hat{i}, \hat{j} = 0, \dots, N_x - 1$ associated with N_x points on the interval $[0, L_x]$. Expressed as a matrix-vector product, the spatial derivative D_x reads

$$D_x \bar{E} = \begin{bmatrix} \hat{D}_x & & & \\ & \hat{D}_x & & \\ & & \ddots & \\ & & & \hat{D}_x \end{bmatrix} \bar{E}. \quad (41)$$

\hat{D}_x is applied to each row $[\bar{E}_{0j}, \bar{E}_{1j}, \dots, \bar{E}_{N_x-1j}]^T$, $j = 0, \dots, N_y - 1$, in the computational grid of Figure 1. To compute the derivative with respect to y , one applies the corresponding one-dimensional $N_y \times N_y$ matrix \hat{D}_y to each column $[\bar{E}_{i0}, \bar{E}_{i1}, \dots, \bar{E}_{iN_y-1}]^T$, $i = 0, \dots, N_x - 1$. This can be conveniently expressed as $D_x = I \otimes \hat{D}_x$ and $D_y = \hat{D}_y \otimes I$ using the tensor product \otimes defined in [5]. Let $A = [a_{\hat{i}\hat{j}}]$ and $B = [b_{\hat{i}\hat{j}}]$ be $k \times l$ and $m \times n$ matrices, respectively. Then their tensor product is given in block matrix form as

$$A \otimes B = \begin{bmatrix} a_{11}B & a_{12}B & \cdots & a_{1l}B \\ a_{21}B & a_{22}B & \cdots & a_{2l}B \\ \vdots & \vdots & & \vdots \\ a_{k1}B & a_{k2}B & \cdots & a_{kl}B \end{bmatrix}. \quad (42)$$

2.2.2 Computations

We obtained computational results using the Fourier pseudospectral time-domain (PSTD) method (30), specifically, we examined snapshots and frequency-domain field distributions of the field components E_x and E_y in a local domain $\Omega = [640, 896] \times [128, 384] \text{ nm}^2$, the region within the dotted line in Figure 1. We used modulated Blackman-Harris pulses [9] covering the range of frequencies $[\frac{c}{\lambda_0} - a, \frac{c}{\lambda_0} + a] \text{ Hz}$, where $a = 1.800\text{e}14$, $\lambda_0 = 340 \text{ nm}$ for snapshots, and $[\frac{c}{\lambda_0} - b, \frac{c}{\lambda_0} + b] \text{ Hz}$, where $b = 7.365\text{e}14$, $\lambda_0 = 340 \text{ nm}$ for frequency-domain simulations. Note that, for the snapshots, because of a hard line source used in the simulation, the pulse width and the time must be chosen so that retro-reflected waves from the line-source cannot get into the local domain Ω . For the frequency-domain field distributions, the pulse width should be short enough to avoid retro-reflected waves from the source getting into the local domain Ω , and the total physical simulation time must be chosen so that the fields go to zero at the end of simulation, avoiding a time-window effect.

The snapshots for the field components E_x and E_y are shown in Figures 5–8. The frequency-domain field distributions for E_x and E_y with compact line source [20] at the sinusoidal frequency $w_0 = \frac{2\pi c}{\lambda_0} \text{ Hz}$ are shown in Figures 9–14. Snapshots at time $11.48\text{e-}15 \text{ sec}$ with $\Delta t = 1.3514\text{e-}18$ require 8,495 iterations in time and a total CPU time of 2987.2 sec on a Mac G5 machine for $N_x = 1024, N_y = 512$. Frequency-domain field distributions with the same size of Δt and 22,200 iterations require a total CPU time of 7893.9 sec.

However, we observe nonphysical oscillations in the PSTD solutions throughout Figures 5–14. In our problem configuration, the solution is piecewise smooth as a result of the discontinuity in the dielectric function along the interface of the cylinder. Hence, we can obtain an accurate approximate solution with the standard Fourier pseudospectral method, although that is a good method for analytic and periodic functions. In the next sections, we introduce a cost-effective reconstruction technique as a postprocessing method and use it to reduce the nonphysical oscillations in our PSTD solutions.

3 Gegenbauer Reconstructions in Finite Spaces

Although the results by Fourier pseudospectral time-domain simulations in the left columns of Figures 5–14 are obscured by oscillations arising from the Gibbs phenomenon, one can recover accurate reconstructions by using either Fourier-Padé approximations [23] or Gegenbauer polynomials [15], [22].

Here, we consider Gegenbauer reconstructions. This method requires a priori knowledge of the location of the discontinuity. In the present application, the discontinuity location, which arises from the jump in dielectric function, is specified as part of the problem definition and Gegenbauer reconstruction is therefore appropriate.

3.1 Gibbs Phenomenon

We briefly revisit the prototype problem on Gibbs oscillation. Consider a nonperiodic analytic function $f(x)$ in $[-1, 1]$. Now, assume that the point values $f(x_j)$, where $x_j = 2j/N, j = 0, \dots, N - 1$, are known but the function $f(x)$ is not. This is equivalent to knowing the first N discrete Fourier coefficients \tilde{f}_k , $-N/2 \leq k \leq N/2 - 1$, of the function $f(x)$ defined by

$$\tilde{f}_k = \sum_{j=0}^{N-1} f(x_j) e^{-i\pi k x_j}. \quad (43)$$

Then the classical Fourier sum

$$f_N(x) = \sum_{k=-N/2}^{N/2-1} \tilde{f}_k e^{i\pi k x} \quad (44)$$

reconstructs the point values everywhere in $-1 \leq x \leq 1$.

The finite Fourier expansion converges exponentially as N increases when the approximated function is analytic (i.e., infinitely smooth) and periodic [13]. If $f(x)$ is either discontinuous or nonperiodic, however, then $f_N(x)$ is not a good approximation to $f(x)$. Away from the discontinuity or the boundary, the

convergence is only $O(\frac{1}{N})$, and there is an overshoot close to the discontinuity or the boundary that does not diminish with increasing N [13]; this is referred to as the Gibbs phenomenon [11]. The phenomenon manifests itself in many situations, including the problem we present in this paper.

3.2 Review of Gegenbauer Approximations

Gottlieb and Shu showed that, knowing the first N Fourier coefficients, one can reconstruct a *rapidly converging* series based on the expansions in Gegenbauer polynomials [15]. The point values of $f(x)$ everywhere in $-1 \leq x \leq 1$ can be recovered with exponential accuracy in the maximum norm up to the discontinuity or the boundary.

The Gegenbauer series for the function $f(x)$, based on the Gegenbauer polynomials $C_n^\alpha(x)$, which are orthogonal over the range $x \in [-1, 1]$ with the weight function $(1-x^2)^{\alpha-\frac{1}{2}}$ for any constant $\alpha \geq 0$, is defined by

$$f(x) = \sum_{n=0}^{\infty} \hat{b}_n^\alpha C_n^\alpha(x), \quad (45)$$

where

$$\hat{b}_n^\alpha = \frac{1}{h_n^\alpha} \int_{-1}^1 (1-x^2)^{\alpha-\frac{1}{2}} C_n^\alpha(x) f(x) dx, \quad (46)$$

with the normalization constant

$$h_n^\alpha = \pi^{\frac{1}{2}} C_n^\alpha(1) \frac{\Gamma(\alpha + \frac{1}{2})}{\Gamma(\alpha)(n + \alpha)} \quad \text{and} \quad C_n^\alpha(1) = \frac{\Gamma(n + 2\alpha)}{n! \Gamma(2\alpha)}. \quad (47)$$

The Gegenbauer polynomials can be expressed by Rodrigues's formula [1], and more conventionally they can be computed by the following recurrence formula [1]:

$$nC_n^\alpha(x) = 2(n + \alpha - 1)x C_{n-1}^\alpha(x) - (n + 2\alpha - 2)C_{n-2}^\alpha(x). \quad (48)$$

They achieve their maximum at the boundary

$$|C_n^\alpha(x)| \leq |C_n^\alpha(1)|, \quad -1 \leq x \leq 1. \quad (49)$$

For large α and n , h_n^α and $C_n^\alpha(1)$ are almost of the same size, which is proven by using Stirling's formula [1], [14]. In Figure 2, Gegenbauer polynomials of degree 5 are shown for different α . As α increases, the amplitude of $C_5^\alpha(x)$ dramatically increases at the boundary. On the other hand, the weight functions rapidly approach zero as α increases. Thus one can see intuitively that $|\hat{b}_n^\alpha|$ is decaying at a rate proportional to the integration of a narrowizing weight function multiplied by $|f(x)|$ as n and α increase. The convergence rate of the infinite series depends on the rate of decay in the magnitude of the coefficients. A rigorous proof of the exponential convergence of the Gegenbauer series to an analytic function $f(x)$ is shown in [18].

Note that more commonly used Chebyshev and Legendre polynomials are important subclasses of the Gegenbauer polynomials with the relations

$$T_n(x) = n \lim_{\alpha \rightarrow 0} \Gamma(2\alpha) C_n^\alpha(x), \quad L_n(x) = C_n^{\frac{1}{2}}(x), \quad (50)$$

where $T_n(x)$ and $L_n(x)$ represent Chebyshev and Legendre polynomials of degree n , respectively. Figure 2 shows some profiles of them for degree $n = 1, 2, \dots, 5$. They are obtained by using a cost-effective version for computing the Gegenbauer polynomials; this method is discussed in section 3 and 4. For computation of the Chebyshev polynomials, following the relation in (50), α is chosen as 1.0e-11 for the limit relation, which gives accuracy to 7 digits.

The truncated Gegenbauer expansion, denoted by

$$g_M^\alpha(x) = \sum_{n=0}^M \hat{b}_n^\alpha C_n^\alpha(x), \quad (51)$$

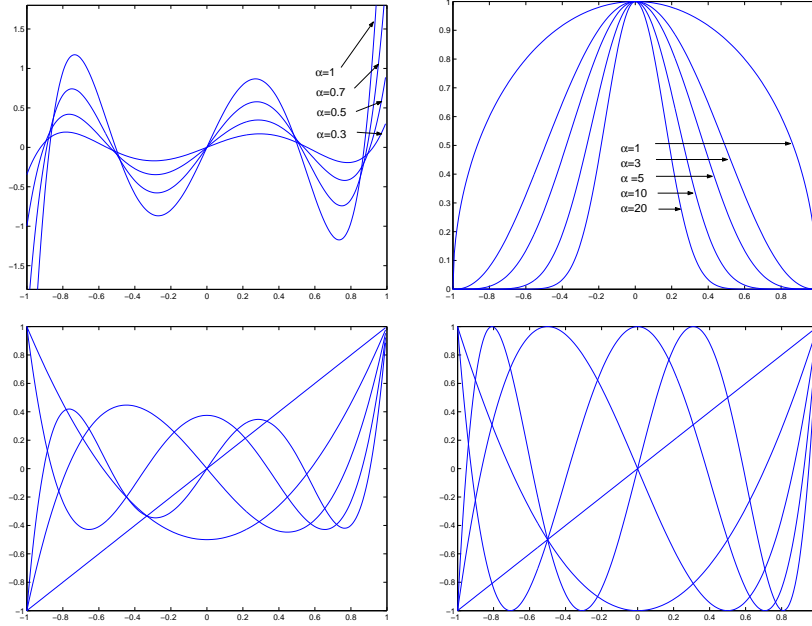


Figure 2: First row: Gegenbauer polynomials $C_5^\alpha(x)$ (left) and weight functions $(1-x^2)^{\alpha-\frac{1}{2}}$ (right) for various α . Second row: Subclasses of Gegenbauer polynomials, Legendre polynomials $L_n(x)$ (left) and Chebyshev polynomials $T_n(x)$ (right) for $n = 1, 2, \dots, 5$.

converges exponentially to an analytic function $f(x)$ in $[-1, 1]$. In practice, however, \hat{b}_n^α must be computed and we are given only an approximation of $f(x)$, the Fourier pseudospectral data, in our problem. It was shown that the Fourier finite expansion (44) can be used to approximate \hat{b}_n^α . We define the discrete Gegenbauer coefficients b_n^α , instead of the continuous Gegenbauer coefficients \hat{b}_n^α , by substituting $f(x)$ by $f_N(x)$ in (46). The discrete Gegenbauer finite expansion is written as

$$g_{M,N}^\alpha(x) = \sum_{n=0}^M b_n^\alpha C_n^\alpha(x), \quad (52)$$

where

$$b_n^\alpha = \frac{1}{h_n^\alpha} \int_{-1}^1 (1-x^2)^{\alpha-\frac{1}{2}} C_n^\alpha(x) f_N(x) dx. \quad (53)$$

Plugging (44) into (53), one obtains

$$b_n^\alpha = \sum_{k=-\frac{N}{2}}^{\frac{N}{2}-1} \tilde{f}_k \left(\frac{1}{h_n^\alpha} \int_{-1}^1 (1-x^2)^{\alpha-\frac{1}{2}} C_n^\alpha(x) e^{i\pi kx} dx \right), \quad (54)$$

where the integration part has an explicit form [3] for $k \neq 0$ as

$$\frac{1}{h_n^\alpha} \int_{-1}^1 (1-x^2)^{\alpha-\frac{1}{2}} C_n^\alpha(x) e^{i\pi kx} dx = \Gamma(\alpha) \left(\frac{2}{k\pi} \right)^\alpha i^n (n+\alpha) J_{n+\alpha}(k\pi), \quad (55)$$

where $\Gamma(x)$ is the gamma function and $J_n(x)$ is the Bessel function of first kind.

To obtain the proof of exponential convergence of $g_{M,N}^\alpha$ to f , we make the following error

$$\|f - g_{M,N}^\alpha\| \leq \|f - g_M^\alpha\| + \|g_M^\alpha - g_{M,N}^\alpha\|, \quad (56)$$

to be exponentially small by showing the two terms on the right-hand side, separately. The *truncation error* is

$$\|g_M^\alpha - g_{M,N}^\alpha\| = \max_{-1 \leq x \leq 1} \left| \sum_{n=0}^M (\hat{b}_n^\alpha - b_n^\alpha) C_n^\alpha(x) \right|, \quad (57)$$

which is exponentially small in maximum norm over $[-1, 1]$ if *both* λ and M grow linearly with N . The *regularization error*

$$\|f - g_M^\alpha\| = \max_{-1 \leq x \leq 1} \left| f(x) - \sum_{n=0}^M \hat{b}_n^\alpha C_n^\alpha(x) \right| \quad (58)$$

is again exponentially small for $\lambda = \gamma m$ with any positive constant γ . Therefore the maximum error for the approximation $g_{M,N}^\alpha$ to $f(x)$ is exponentially small. The detailed proof of exponential convergence is shown in [15].

The suggested procedure to obtain the discrete Gegenbauer finite expansion $g_{M,N}^\alpha$ generally consists of the following steps:

Step 1. Compute the first $M + 1$ discrete Gegenbauer coefficients b_n^α in (54) using $f_N(x)$.

Step 2. Construct the series (52) cost-effectively by expressing the Gegenbauer polynomials in terms of trigonometric functions.

In the next sections, we first discuss the detailed procedure for single-domain and multidomain reconstruction in one dimension, and then extend to two dimensions.

3.3 Single-Domain Reconstruction

Here, we focus on a cost-effective Gegenbauer reconstruction to compute $g_{M,N}^\alpha$ for a single domain on $[-1, 1]$. Let us define the following notation for formula (55) :

$$\begin{aligned} \text{For } k \neq 0, \quad B_{n,k} &= \Gamma(\alpha) \left(\frac{2}{k\pi}\right)^\alpha i^n (n + \alpha) J_{n+\alpha}(k\pi), \\ \text{For } k = 0, \quad B_{n,k} &= \delta_{nk}. \end{aligned} \quad (59)$$

Then the discrete Gegenbauer coefficients b_n^α in (54) can be written in matrix form as

$$\begin{bmatrix} b_0^\alpha \\ b_1^\alpha \\ \vdots \\ b_M^\alpha \end{bmatrix} = \begin{bmatrix} B_{0,-\frac{N}{2}} & B_{0,-\frac{N}{2}+1} & \cdots & B_{0,\frac{N}{2}-1} \\ B_{1,-\frac{N}{2}} & B_{1,-\frac{N}{2}+1} & \cdots & B_{1,\frac{N}{2}-1} \\ \vdots & \vdots & \cdots & \vdots \\ B_{M,-\frac{N}{2}} & B_{M,-\frac{N}{2}+1} & \cdots & B_{M,\frac{N}{2}-1} \end{bmatrix} \begin{bmatrix} \tilde{f}_{-\frac{N}{2}} \\ \tilde{f}_{-\frac{N}{2}+1} \\ \vdots \\ \tilde{f}_{\frac{N}{2}-1} \end{bmatrix}.$$

Applying the even and odd property of the Bessel function, we have $B_{n,k} = \overline{B_{n,-k}}$. For a real function $f(x)$, the Fourier coefficients are $\tilde{f}_k = \overline{\tilde{f}_{-k}}$. Thus we have

$$\begin{aligned} b_n^\alpha &= B_{n,-\frac{N}{2}} \tilde{f}_{-\frac{N}{2}} + \sum_{k=-(\frac{N}{2}-1)}^{-1} B_{n,k} \tilde{f}_k + B_{0,0} \tilde{f}_0 + \sum_{k=1}^{\frac{N}{2}-1} B_{n,k} \tilde{f}_k \\ &= B_{n,-\frac{N}{2}} \tilde{f}_{-\frac{N}{2}} + B_{0,0} \tilde{f}_0 + \sum_{k=1}^{\frac{N}{2}-1} (B_{n,k} \tilde{f}_k + \overline{B_{n,k} \tilde{f}_k}). \end{aligned} \quad (60)$$

By taking the conjugate of $(N/2 - 1)$ terms of $B_{n,k} \tilde{f}_k$, we can now reduce the computational cost for computing the Gegenbauer coefficients from $O(N)$ to $O(N/2)$.

Next, following the procedure introduced in [22], we take the explicit form of the Gegenbauer polynomials expanded by the trigonometric polynomials, instead of using the conventional recurrence formula [3] : for $x = \cos \theta \in [-1, 1]$ with $\theta \in [-\pi, \pi]$,

$$C_n^\alpha(\cos \theta) = \sum_{m=0}^n a_{m,n}^\alpha \cos(n - 2m)\theta, \quad (61)$$

where

$$a_{m,n}^\alpha = \frac{\Gamma(\alpha + m)\Gamma(\alpha + n - m)}{m!(n - m)!\Gamma^2(\alpha)}. \quad (62)$$

Let us consider a set of grids $x_i, i = 0, \dots, N - 1$. Then the approximate Gegenbauer expansion on grids x_i is

$$\begin{aligned} g_{M,N}^\alpha(x_i) &= \sum_{n=0}^M b_n^\alpha C_n^\alpha(\cos x_i) \\ &= \sum_{n=0}^M b_n^\alpha \left(\sum_{m=0}^n a_{m,n} \cos[(n - 2m)(\cos^{-1} x_i)] \right). \end{aligned} \quad (63)$$

Let $T_{i,m} = \cos(m\theta_i)$ for $\theta_i = \cos^{-1} x_i$ and $\mathbf{g}_i = g_{M,N}^\alpha(x_i)$. Assuming that M is even for the sake of simplicity, we can express the Gegenbauer reconstruction on the grids x_i in matrix form as follows:

$$\begin{bmatrix} \mathbf{g}_0 \\ \mathbf{g}_1 \\ \vdots \\ \mathbf{g}_{N-1} \end{bmatrix} = \begin{bmatrix} T_{0,0} & T_{0,1} & \dots & T_{0,M} \\ T_{1,0} & T_{1,1} & \dots & T_{1,M} \\ \vdots & \vdots & \dots & \vdots \\ \vdots & \vdots & \dots & \vdots \\ T_{N-1,0} & T_{N-1,1} & \dots & T_{N-1,M} \end{bmatrix} \begin{bmatrix} a_{00}^\alpha & 0 & a_{12}^\alpha & 0 & \dots & a_{\frac{M}{2},M}^\alpha \\ 0 & 2a_{01}^\alpha & 0 & 2a_{13}^\alpha & \dots & 0 \\ 0 & 0 & 2a_{02}^\alpha & 0 & \dots & 0 \\ \vdots & \vdots & 0 & \vdots & \dots & 2a_{1M}^\alpha \\ \vdots & \vdots & \vdots & 0 & \dots & 0 \\ 0 & 0 & 0 & 0 & 0 & 2a_{0M}^\alpha \end{bmatrix} \begin{bmatrix} b_0^\alpha \\ b_1^\alpha \\ \vdots \\ \vdots \\ b_M^\alpha \end{bmatrix}.$$

To discuss the computational cost, we denote the first $N \times (M + 1)$ matrix in the right side of the above equation by \mathbf{T} and the second $(M + 1) \times (M + 1)$ matrix by \mathbf{A} , that is,

$$\mathbf{g} = \mathbf{T}\mathbf{A}\mathbf{b}, \quad (64)$$

where $\mathbf{g} = [\mathbf{g}_0, \mathbf{g}_1, \dots, \mathbf{g}_{N-1}]^T$ and $\mathbf{b} = [b_0^\alpha, b_1^\alpha, \dots, b_M^\alpha]^T$. The number of operations for the matrix-vector multiplication $\mathbf{A}\mathbf{b}$ is $\frac{(M+2)(M+4)}{4}$, and the multiplication with \mathbf{T} is $N(M+1)$. Then, for $M = \beta N$ ($0 < \beta < 1$) (i.e., proportional to N), the total cost is $O(\frac{1}{4}\beta(\beta + 4)N^2)$. On the other hand, the conventional recurrence formula (48) costs $O(3\beta N^2)$. Since $\frac{\beta+4}{4} \approx 1$, the fast version reduces the computational cost by one-third.

In summary, the reconstruction procedure follows the general steps:

Step 1. Compute the first $M + 1$ discrete Gegenbauer coefficients (60).

Step 2. Construct the Gegenbauer finite sum on grids following (64).

Example. We apply the reconstruction technique to Fourier pseudospectral data of a nonperiodic function $f(x) = x$ on $[-1, 1]$, assuming that we are given $N = 128$ discrete Fourier coefficients, as defined in (43), on the grids $x_i = -1 + 2i/N, i = 0, \dots, N - 1$. Figure 2 shows the Fourier approximation with $N = 128$ modes, its reconstructed results, and their pointwise errors. Since the function $f(x)$ is nonperiodic, the standard Fourier method gives only $O(\frac{1}{N})$ and $O(1)$ convergence, and oscillations are severe near the boundary. Since $f_N(x_i)$ is exact with $f(x_i)$ on grids x_i , the point values are evaluated on $y_i = -1 + i/N, i = 0, \dots, 2N - 1$ in order to see the oscillations and their resolution clearly. After reconstruction with the parameters $m = 4, \alpha = 3$ the result recovers the original function $f(x) = x$ successfully. As the parameters increase to $m = 8, \alpha = 6$, the errors drop exponentially up to the boundary. Reconstruction CPU times are provided.

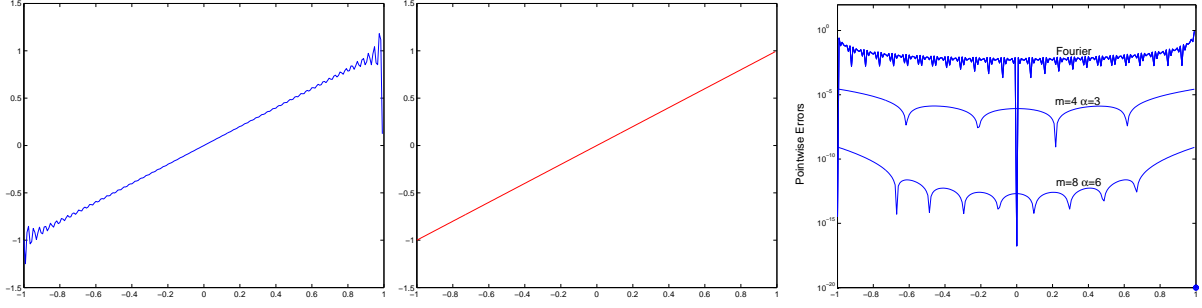


Figure 3: From the left: Fourier approximation, its Gegenbauer reconstruction, and pointwise errors. Reconstruction CPU time = 0.22 sec and 0.42 sec for $m = 4, \alpha = 3$ and $m = 8, \alpha = 6$, respectively, on an AMD Athlon of 1 GHz.

3.4 Multidomain Reconstruction

Consider a piecewise analytic function $f(x)$ that is integrable in $[0, L]$. Suppose that $f(x)$ has known discontinuities at $x = d_0$ and $x = d_1$ in $[0, L]$. Then we divide the global domain into three subdomains, denoted by $\Omega_1 = [0, d_0]$, $\Omega_2 = [d_0, d_1]$, and $\Omega_3 = [d_1, L]$, and carry out the Gegenbauer reconstruction in each subdomain. First, we define a set of grids in the global domain defined by $x_j = \frac{Lj}{N}$, $j = 0, 1, \dots, N-1$ and assume that the point values $f(x_j)$ ($j = 0, 1, \dots, N-1$) are given. Then we obtain the Fourier coefficients \tilde{f}_k ($-\frac{N}{2} \leq k \leq \frac{N}{2} - 1$) by applying a discrete fast Fourier transform, so that the classical Fourier finite sum everywhere in $[0, L]$ is

$$f_N(x) = \sum_{k=-\frac{N}{2}}^{\frac{N}{2}-1} \tilde{f}_k e^{i\frac{2\pi k}{L}x}. \quad (65)$$

Let us denote a subdomain by $\Omega_s = [a, b]$ and define a local variable, for $\xi \in [-1, 1]$, $x^s = \frac{(b-a)}{2}\xi + \frac{(b+a)}{2}$. Let $\epsilon = \frac{b-a}{L}$ and $\delta = \frac{b+a}{L}$. The Fourier finite sum using the variable ξ is

$$f_N(x(\xi)) = \sum_{k=-\frac{N}{2}}^{\frac{N}{2}-1} \tilde{f}_k e^{i\pi k(\epsilon\xi + \delta)}. \quad (66)$$

Now we define the Gegenbauer coefficients in each subdomain:

$$b_n^{\Omega_s} = \frac{1}{h_n^\alpha} \int_{-1}^1 (1 - \xi^2)^{\alpha - \frac{1}{2}} C_n^\alpha(\xi) f_N(x(\xi)) d\xi. \quad (67)$$

Then plugging (66) into (67) and using the explicit formula (55) for the integration part, we denote

$$\begin{aligned} \text{For } k \neq 0, \quad B_{n,k}^{\Omega_s} &= \frac{e^{i\pi k\delta}}{h_n^\alpha} \int_{-1}^1 (1 - \xi^2)^{\alpha - \frac{1}{2}} C_n^\alpha(\xi) e^{i\pi k\epsilon\xi} d\xi \\ &= e^{i\pi k\delta} \Gamma(\alpha) \left(\frac{2}{k\pi\epsilon}\right)^\alpha i^n (n + \alpha) J_{n+\alpha}(k\epsilon\pi), \\ \text{For } k = 0, \quad B_{n,k}^{\Omega_s} &= \delta_{nk}. \end{aligned} \quad (68)$$

Then, the local Gegenbauer coefficients are expressed in a matrix form

$$\begin{bmatrix} b_0^{\Omega_s} \\ b_1^{\Omega_s} \\ \vdots \\ b_M^{\Omega_s} \end{bmatrix} = \begin{bmatrix} B_{0,-\frac{N}{2}}^{\Omega_s} & B_{0,-\frac{N}{2}+1}^{\Omega_s} & \cdots & B_{0,\frac{N}{2}-1}^{\Omega_s} \\ B_{1,-\frac{N}{2}}^{\Omega_s} & B_{1,-\frac{N}{2}+1}^{\Omega_s} & \cdots & B_{1,\frac{N}{2}-1}^{\Omega_s} \\ \vdots & \vdots & \cdots & \vdots \\ B_{M,-\frac{N}{2}}^{\Omega_s} & B_{M,-\frac{N}{2}+1}^{\Omega_s} & \cdots & B_{M,\frac{N}{2}-1}^{\Omega_s} \end{bmatrix} \begin{bmatrix} \tilde{f}_{-\frac{N}{2}} \\ \tilde{f}_{-\frac{N}{2}+1} \\ \vdots \\ \tilde{f}_{\frac{N}{2}-1} \end{bmatrix}.$$

Next, we evaluate the point values in each subdomain as follows. Let $\mathbf{x}^s = \{x_i^s, \dots, x_j^s\}$ be a subset of $\{x_j\}_{j=0}^{N-1}$, which is in Ω_s . Define $T_{i,m}^s = \cos[m(\cos^{-1} \xi_i)]$ for $\xi_i = \frac{2}{b-a}x_i^s - \frac{b+a}{b-a}$. Note that the Gegenbauer coefficients are newly computed in each subdomain and the reconstructed point values, denoted by $\mathbf{g}_i^{\Omega_s}$, on grid set \mathbf{x}^s in each subdomain are obtained by

$$\begin{bmatrix} \mathbf{g}_i^{\Omega_s} \\ \vdots \\ \mathbf{g}_j^{\Omega_s} \end{bmatrix} = \begin{bmatrix} T_{i,0}^s & T_{i,1}^s & \cdots & T_{i,M}^s \\ \vdots & \vdots & \cdots & \vdots \\ \vdots & \vdots & \cdots & \vdots \\ T_{j,0}^s & T_{j,1}^s & \cdots & T_{j,M}^s \end{bmatrix} \begin{bmatrix} a_{00} & 0 & a_{12} & 0 & \cdots & a_{\frac{M}{2},M} \\ 0 & 2a_{01} & 0 & 2a_{13} & \cdots & 0 \\ 0 & 0 & 2a_{02} & 0 & \cdots & 0 \\ \vdots & \vdots & 0 & \vdots & \cdots & 2a_{1M} \\ \vdots & \vdots & \vdots & 0 & \cdots & 0 \\ 0 & 0 & 0 & 0 & 0 & 2a_{0M} \end{bmatrix} \begin{bmatrix} b_0^{\Omega_s} \\ b_1^{\Omega_s} \\ \vdots \\ b_M^{\Omega_s} \end{bmatrix}.$$

Let N^s be the number of the elements in \mathbf{x}^s and the number of discontinuities D . Then the first $N^s \times (M+1)$ matrix in the right-hand side of the equation above is denoted by \mathbf{T}^s and the second $(M+1) \times (M+1)$ matrix by \mathbf{A}^s . Then

$$\mathbf{g}^s = \mathbf{T}^s \mathbf{A}^s \mathbf{b}^s, \quad (69)$$

where $\mathbf{g}^s = [g_i^{\Omega_s}, \dots, g_j^{\Omega_s}]^T$ and $\mathbf{b}^s = [b_0^{\Omega_s}, b_1^{\Omega_s}, \dots, b_M^{\Omega_s}]^T$. The number of operations for the matrix-vector multiplication $\mathbf{A}^s \mathbf{b}^s$ is $\frac{(M+2)(M+4)}{4}$. However, one has to compute this procedure for each subdomain, so the total of amount for this procedure is $\frac{D(M+2)(M+4)}{4}$. The multiplication with \mathbf{T}^s is $N^s(M+1)$ in each subdomain; however, it remains the same amount of work as in the single-domain case, so $N(M+1)$. Thus, for $M = \beta N$ ($0 < \beta < 1$) (i.e., proportional to N), the total cost is $O(\frac{1}{4}\beta(D\beta+4)N^2)$. On the other hand, the conventional recurrence formula costs $O(3D\beta N^2)$.

In summary, the reconstruction procedure for multidomain case is as follows :

- Step 1. Compute the first $M+1$ discrete Gegenbauer coefficients (67) in a subdomain.
- Step 2. Construct the Gegenbauer finite sum (69) on the grids in the subdomain.
- Step 3. Repeat Step 1 and Step 2 in the remaining subdomains, separately.

Examples. Consider the following discontinuous functions, and assume that we are given only $N = 128$ discrete Fourier coefficients, as defined in (43), for each function.

$$f_1(x) = \begin{cases} x+1 & (-1 \leq x \leq 0) \\ x-1 & (0 \leq x \leq 1) \end{cases} \quad \text{and} \quad f_2(x) = \begin{cases} x^3 - x^2 + 2 & (-1 \leq x \leq -\frac{1}{2}) \\ x^2 + 5 & (-\frac{1}{2} \leq x \leq \frac{1}{2}) \\ x^3 - 2 & (\frac{1}{2} \leq x \leq 1). \end{cases} \quad (70)$$

Figure 3 shows the Fourier approximations with $N = 128$, their reconstructed results and the pointwise errors for the functions. For discontinuous functions, the standard Fourier approximation gives only $O(\frac{1}{N})$ convergence away from the discontinuities and $O(1)$ convergence near the discontinuities, as shown in the error plot. Reconstructions are carried out for the function $f_1(x)$ with two subdomains and for the function $f_2(x)$ with three subdomains. For the reconstructed ones with increasing parameters, the errors drop exponentially up to discontinuities.

4 Two-Dimensional Reconstruction

In this section, we extend the use of the cost-effective version of the Gegenbauer reconstruction technique to two-dimensional problems.

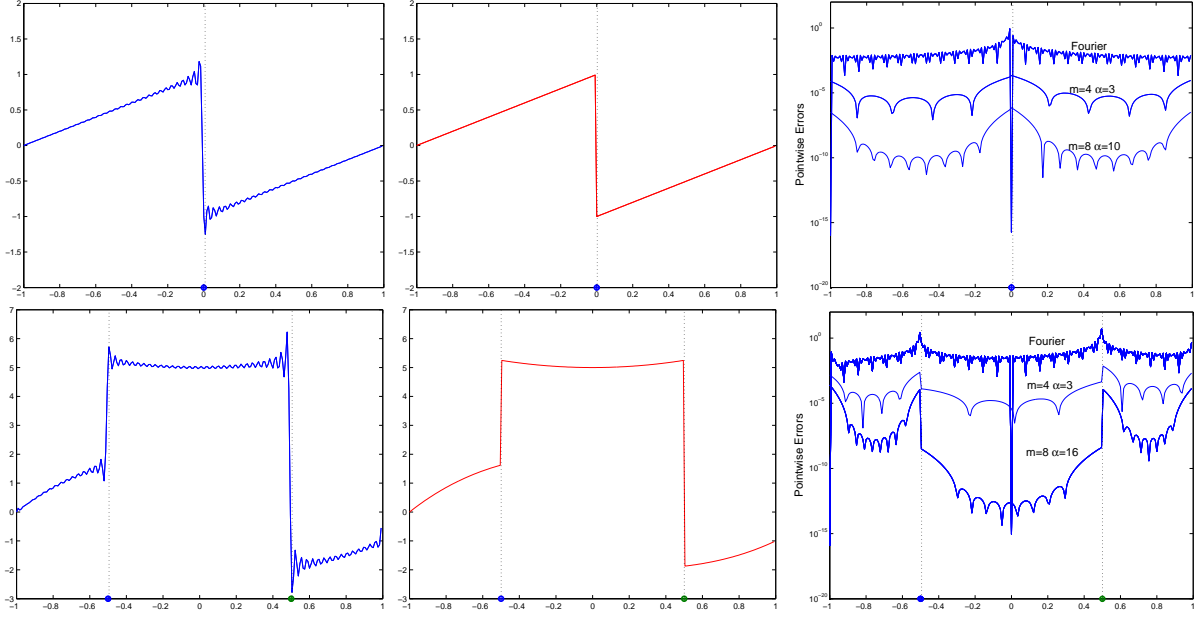


Figure 4: From the left columns: Fourier approximations, their Gegenbauer reconstructions, and pointwise errors. Reconstruction CPU time: 0.47 sec ($m = 4, \alpha = 3$) and 0.90 sec ($m = 8, \alpha = 10$) for $f_1(x)$, and 0.72 sec ($m = 4, \alpha = 3$) and 1.38 sec ($m = 8, \alpha = 16$) for $f_2(x)$ on an AMD Athlon of 1 GHz.

4.1 Global Domain $[-1, 1]^2$

The Gegenbauer finite sum in two dimensions has the following form. For $x = \cos \theta, y = \cos \eta$ in a domain $\Omega = [-1, 1]^2$, denoting $\alpha = (\alpha_x, \alpha_y)$ and $M = (M_x, M_y)$, we have

$$g_{M,N}^\alpha(x, y) = \sum_{n=0}^{M_x} \sum_{l=0}^{M_y} b_{n,l}^\alpha C_n^{\alpha_x}(x) C_l^{\alpha_y}(y), \quad (71)$$

where

$$C_n^\alpha(\cos \theta) = \sum_{m=0}^n a_{m,n}^\alpha \cos(n - 2m)\theta, \quad (72)$$

and

$$a_{m,n}^\alpha = \frac{\Gamma(\alpha + m)\Gamma(\alpha + n - m)}{m!(n - m)!\Gamma^2(\alpha)}, \quad (73)$$

where Γ is the gamma function. The coefficients $b_{n,l}^\alpha$ for the Gegenbauer finite sum in two dimensions are defined by

$$b_{n,l}^\alpha = \frac{1}{h_n^{\alpha_x} h_l^{\alpha_y}} \int_{-1}^1 \int_{-1}^1 (1 - x^2)^{\alpha_x - \frac{1}{2}} (1 - y^2)^{\alpha_y - \frac{1}{2}} C_n^{\alpha_x}(x) C_l^{\alpha_y}(y) f_N(x, y) dx dy. \quad (74)$$

4.2 Subdomains $\Omega_s = [a_x, b_x] \times [a_y, b_y] \subset [0, L]^2$

Consider the computational domain $[0, L]^2$. Define a set of grids $x_i = \frac{L i}{N_x} (i = 0, \dots, N_x - 1)$ and $y_j = \frac{L j}{N_y} (j = 0, \dots, N_y - 1)$. Now, assume that the point values $f(x_i, y_j)$ are known but the function $f(x, y)$ is not. Then

the discrete Fourier coefficients \tilde{f}_{k_x, k_y} , $-\frac{N}{2} \leq k_x, k_y \leq \frac{N}{2} - 1$ are obtained by

$$\tilde{f}_{k_x, k_y} = \sum_{i=0}^{N-1} \sum_{j=0}^{N-1} f(x_i, y_j) e^{-i \frac{2\pi k_x}{L} x_i} e^{-i \frac{2\pi k_y}{L} y_j}, \quad (75)$$

and the two-dimensional Fourier finite sum everywhere in $\Omega = [0, L]^2$ is

$$f_N(x, y) = \sum_{k_x = -\frac{N}{2}}^{\frac{N}{2}-1} \sum_{k_y = -\frac{N}{2}}^{\frac{N}{2}-1} \tilde{f}_{k_x, k_y} e^{i \frac{2\pi k_x}{L} x} e^{i \frac{2\pi k_y}{L} y}. \quad (76)$$

Let us denote a subdomain by $\Omega_{s,t} = [a_x, b_x] \times [a_y, b_y]$, where a_x and b_x are the known discontinuities in x -direction and a_y and b_y in y -direction. Define local variables, for $\xi, \eta \in [-1, 1] \times [-1, 1]$, $x^s = \frac{(b_x - a_x)}{2} \xi + \frac{(b_x + a_x)}{2}$ and $y^t = \frac{(b_y - a_y)}{2} \eta + \frac{(b_y + a_y)}{2}$. Let $\epsilon_x = \frac{b_x - a_x}{L}$, $\delta_x = \frac{b_x + a_x}{L}$, $\epsilon_y = \frac{b_y - a_y}{L}$ and $\delta_y = \frac{b_y + a_y}{L}$. Then the Fourier finite sum in the subdomain Ω_s is expressed by

$$f_N(x^s(\xi), y^t(\eta)) = \sum_{k_x = -\frac{N}{2}}^{\frac{N}{2}-1} \sum_{k_y = -\frac{N}{2}}^{\frac{N}{2}-1} \tilde{f}_{k_x, k_y} e^{i\pi k_x (\epsilon_x \xi + \delta_x)} e^{i\pi k_y (\epsilon_y \eta + \delta_y)}. \quad (77)$$

Plugging (75) into (77), we have

$$\begin{aligned} f_N(x^s(\xi), y^t(\eta)) &= \sum_{k_y = -\frac{N}{2}}^{\frac{N}{2}-1} \sum_{j=0}^{N-1} \left[\sum_{k_x = -\frac{N}{2}}^{\frac{N}{2}-1} \left(\sum_{i=0}^{N-1} f(x_i, y_j) e^{-i \frac{2\pi k_x}{L} x_i} \right) e^{i\pi k_x x^s(\xi)} \right] e^{-i \frac{2\pi k_y}{L} y_j} e^{i\pi k_y y^t(\eta)} \\ &= \sum_{k_y = -\frac{N}{2}}^{\frac{N}{2}-1} \left(\sum_{j=0}^{N-1} f_N(x^s(\xi), y_j) e^{-i \frac{2\pi k_y}{L} y_j} \right) e^{i\pi k_y y^t(\eta)}, \end{aligned} \quad (78)$$

and the Gegenbauer coefficients in the subdomain Ω_s have the following form

$$b_{n,l}^{\Omega_{s,t}} = \frac{1}{h_l^{\alpha_y}} \int_{-1}^1 (1-y^2)^{\alpha_y - \frac{1}{2}} C_l^{\alpha_y}(\eta) \left[\sum_{k_y = -\frac{N}{2}}^{\frac{N}{2}-1} \left(\sum_{j=0}^{N-1} \mathbf{b}_l^{\Omega_s}(n, y_j) e^{-i \frac{2\pi k_y}{L} y_j} \right) e^{i\pi k_y y^t(\eta)} \right] d\eta, \quad (79)$$

where

$$\mathbf{b}_l^{\Omega_s}(n, y_j) = \frac{1}{h_l^{\alpha_x}} \int_{-1}^1 (1-\xi^2)^{\alpha_x - \frac{1}{2}} C_n^{\alpha_x}(\xi) f_N(x^s(\xi), y_j) d\xi. \quad (80)$$

Then, for a fixed y_j , the one-dimensional Gegenbauer reconstruction in the x -direction is written as

$$\mathbf{g}_l^{\Omega_{s,t}}(x^s(\xi), y_j) = \sum_{n=0}^{M_x} \mathbf{b}_l^{\Omega_s}(n, y_j) C_n^{\alpha_x}(\xi). \quad (81)$$

Finally, the two-dimensional reconstruction form is

$$g^{\Omega_{s,t}}(x^s(\xi), y^t(\eta)) = \sum_{l=0}^{M_y} b_{n,l}^{\Omega_{s,t}} C_l^{\alpha_y}(\eta), \quad (82)$$

where

$$b_{n,l}^{\Omega_{s,t}} = \frac{1}{h_n^{\alpha_y}} \int_{-1}^1 (1-y^2)^{\alpha_y - \frac{1}{2}} C_l^{\alpha_y}(\eta) \left[\sum_{k_y = -\frac{N}{2}}^{\frac{N}{2}-1} \left(\sum_{j=0}^{N-1} \mathbf{g}_l^{\Omega_{s,t}}(x^s(\xi), y_j) e^{-i \frac{2\pi k_y}{L} y_j} \right) e^{i\pi k_y y^t(\eta)} \right] d\eta. \quad (83)$$

Following (68) and (69), the local Gegenbauer coefficients are given in matrix form as

$$b^{\Omega_{s,t}} = \mathbf{B}_y^{\Omega^t} \tilde{\mathbf{f}} \left(\mathbf{B}_x^{\Omega^s} \right)^T, \quad (84)$$

where $b^{\Omega_{s,t}} = [b_{n,l}^{\Omega_{s,t}}]$, $\tilde{\mathbf{f}} = \tilde{f}_{k_y, k_x}$, $\mathbf{B}_x^{\Omega^s} = [B_{n, k_x}^{\Omega^s}]$, and $\mathbf{B}_y^{\Omega^t} = [B_{l, k_y}^{\Omega^t}]$, as defined in (69). Then the two-dimensional Gegenbauer reconstruction can be summarized in matrix form as follows:

$$\mathbf{g}^{s,t} = [\mathbf{T}_y^t \mathbf{A}_y^t (\mathbf{T}_x^s \mathbf{A}_x^s b^{\Omega_{s,t}})^T]^T = \mathbf{T}_x^s \mathbf{A}_x^s (b^{\Omega_{s,t}})^T (\mathbf{A}_y^t)^T (\mathbf{T}_y^t)^T, \quad (85)$$

where $\mathbf{g}^{s,t} = [g_{i,j}^{\Omega_{s,t}}]^T$, $\mathbf{T}_x^s = [T_{i,m}^s] = [\cos(m(\cos^{-1} \xi_i))]$, and $\mathbf{T}_y^t = [T_{j,m}^t] = [\cos(m(\cos^{-1} \eta_j))]$ for $\xi_i = \frac{2}{b_x - a_x} \zeta_i^s - \frac{b_x + a_x}{b_x - a_x}$, and $\eta_j = \frac{2}{b_y - a_y} \eta_j^t - \frac{b_y + a_y}{b_y - a_y}$, respectively.

In actual computation, the reconstruction procedure for the two-dimensional problem can be done through the following steps, which is in fact the one-dimensional reconstruction slice by slice in x direction and then the same procedure through in y direction:

- Step 1. Compute the one-dimensional discrete Fourier coefficients with respect to x for a fixed y_j .
- Step 2. Compute the first $M + 1$ discrete Gegenbauer coefficients in a subdomain.
- Step 3. Construct the Gegenbauer finite sum on the grids in the subdomain.
- Step 4. Repeat Steps 2–3 in the remaining subdomains, separately, for the fixed y_j .
- Step 5. Repeat Steps 1–4 for each y_j , separately, and store all the data for the next step.
- Step 6. Compute the one-dimensional discrete Fourier coefficients with respect to y for a fixed x_i .
- Step 7. Repeat Steps 2–5 for all x_i , separately.

Applications. We apply the cost-effective Gegenbauer reconstruction technique to the two-dimensional Fourier pseudospectral time-domain solutions obtained by (30), shown in the left columns of the Figures 5–14. The reconstructed results are demonstrated in the right columns of Figures 5–14 associated with the PSTD results. Those figures are for the regions within the dotted box in the computational domain shown in Figure 1. The data size in the box is 256×256 in the case of $N_x = 1024$, $N_y = 512$.

The Fourier-pseudospectral solutions show nonphysical oscillations all over the domain across the cylinder and strong oscillations close to the surface of the nanocylinder. Figures 6 and 8 and Figures 12 and 14 show the one-dimensional slices along the specified axes across the cylinder. One-dimensional reconstructions are carried out with five subdomains. Each subdomain takes different parameters m and α during the reconstruction. At this stage, the parameters are chosen by observation through numerical experiments. One- and two-dimensional reconstruction results show a clear improvement in reducing the oscillations.

5 Discussions

Parameter optimization is important for the Gegenbauer reconstruction technique to be useful in practice. In this problem, the regions near the sharp changes of the solutions require relatively larger α and smaller m as in Figures 6 and 8, whereas in the region with relatively smooth changes of the solutions work fine with small α as in Figures 12 and 14. Thus we might have consistent results generally with small α and large m in the smooth region and large α and small m in the subdomain where the solutions are nonsmooth. Accordingly, we introduce an idea to implement an automated reconstruction algorithm, that maybe parameter independent in real computations. Since we know the reconstruction behaviors depending on m and α , we can fix the parameters for a more structured and a relatively smooth region a priori by initially giving the minimum number of the subdomains taking account of the discontinuities. Then we can carry out the reconstructions until they give better resolutions, by increasing the number of subdomains, instead of controlling the resolution by changing the parameters. An a posteriori error estimate is required to measure the improvement of the reconstructed solution. To divide the subdomains, we use the idea of adaptivity; that is, we increase the number of subdomains around the discontinuities. This idea will be further discussed in a future paper.

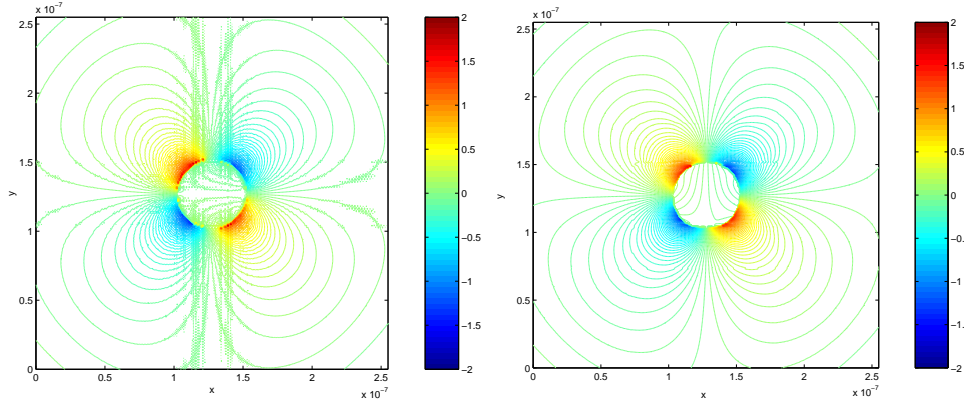


Figure 5: Snapshots of E_x at time = $11.48e-15$ sec with $\Delta t = 1.3514e-18$: From the left, PSTD solution(CPU time= 2987.2 sec on a Mac G5) and Gegenbauer reconstruction (CPU time= 164.40 sec on an AMD Athlon of 1 GHz).

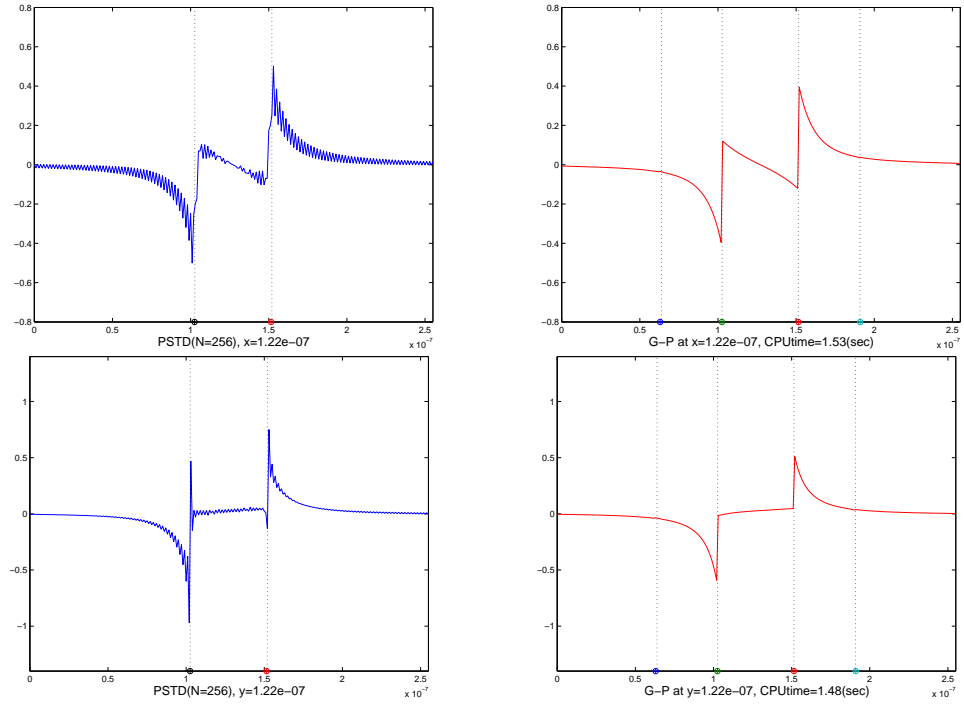


Figure 6: One-dimensional slices of E_x : Dotted lines indicate the interfaces of the cylinder for the spectral (PSTD: left column) solution and the interfaces of subdomains for the Gegenbauer postprocessed (G-P: right column) solution. Parameters for G-P are chosen as $m = 7, 7, 4, 7, 7$ for five subdomains from left to right with a fixed $\alpha = 16$.

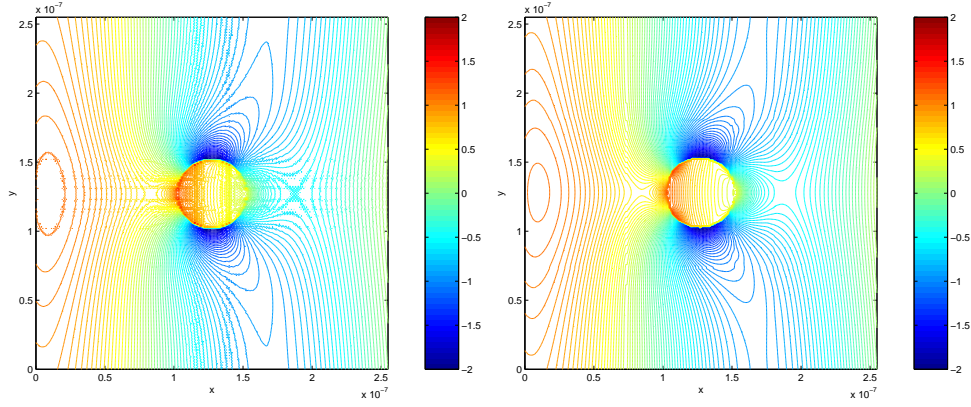


Figure 7: Snapshots of E_y at time = $11.48e-15$ sec with $\Delta t = 1.3514e-18$: From the left, PSTD solution (CPU time= 2987.2 sec on a Mac G5) and Gegenbauer reconstruction (CPU time = 164.79 sec on an AMD Athlon of 1 GHz).

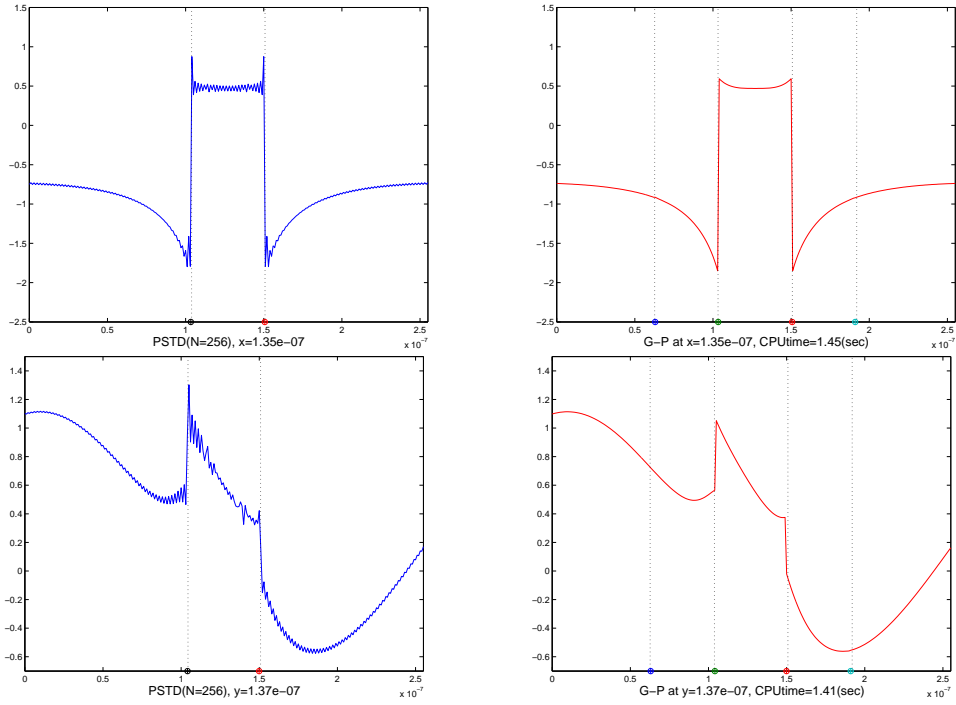


Figure 8: One-dimensional slices of E_y : Dotted lines indicate the interfaces of the cylinder for the spectral (PSTD: left column) solution and the interfaces of subdomains for the Gegenbauer postprocessed (G-P: right column) solution. Parameters for G-P are chosen as $m = 5, 5, 3, 5, 5$ for five subdomains from left to right with a fixed $\alpha = 18$.

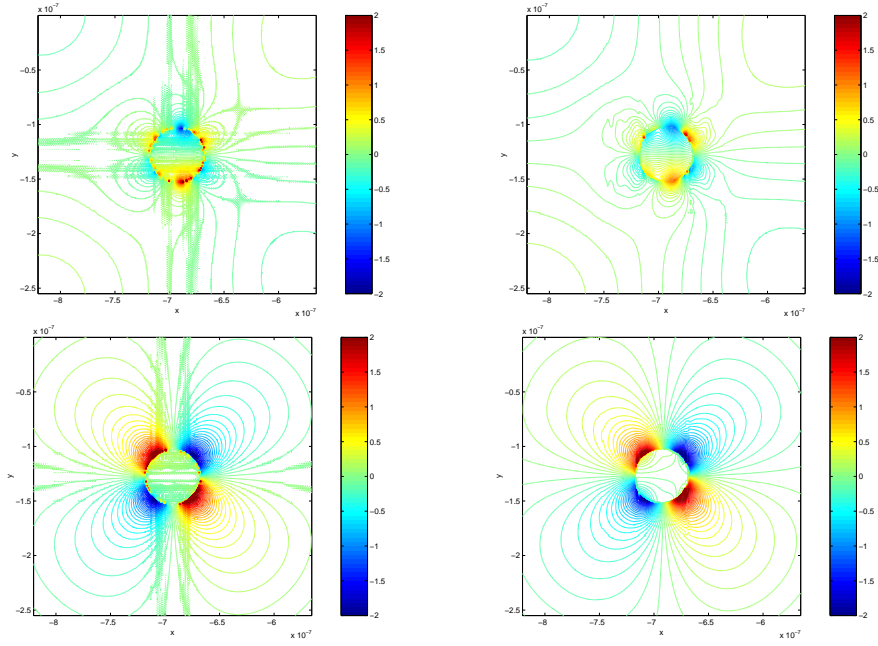


Figure 9: Frequency-domain field distributions of E_x : the real (first row) and imaginary part (second row) of E_x . From the left column: PSTD solutions and their Gegenbauer reconstructions.

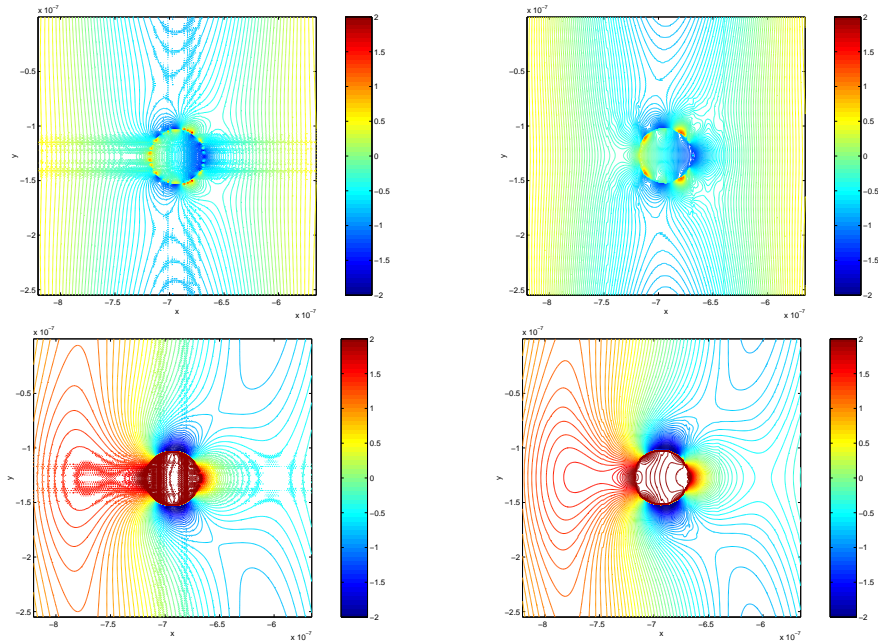


Figure 10: Frequency-domain field distributions of E_y : the real (first row) and imaginary part (second row) of E_y . From the left column: PSTD solutions and their Gegenbauer reconstructions.

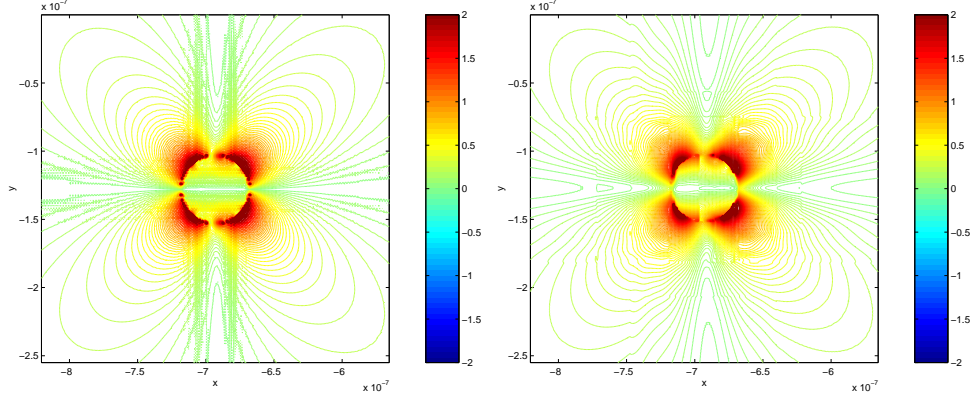


Figure 11: Frequency-domain field distribution of $|E_x|$. $\Delta t = 1.3514e-18$. From the left: PSTD solution (CPU time= 7893.9 sec on a Mac G5) and its Gegenbauer reconstruction (CPU time = 178.91 sec on an AMD Athlon of 1 GHz).

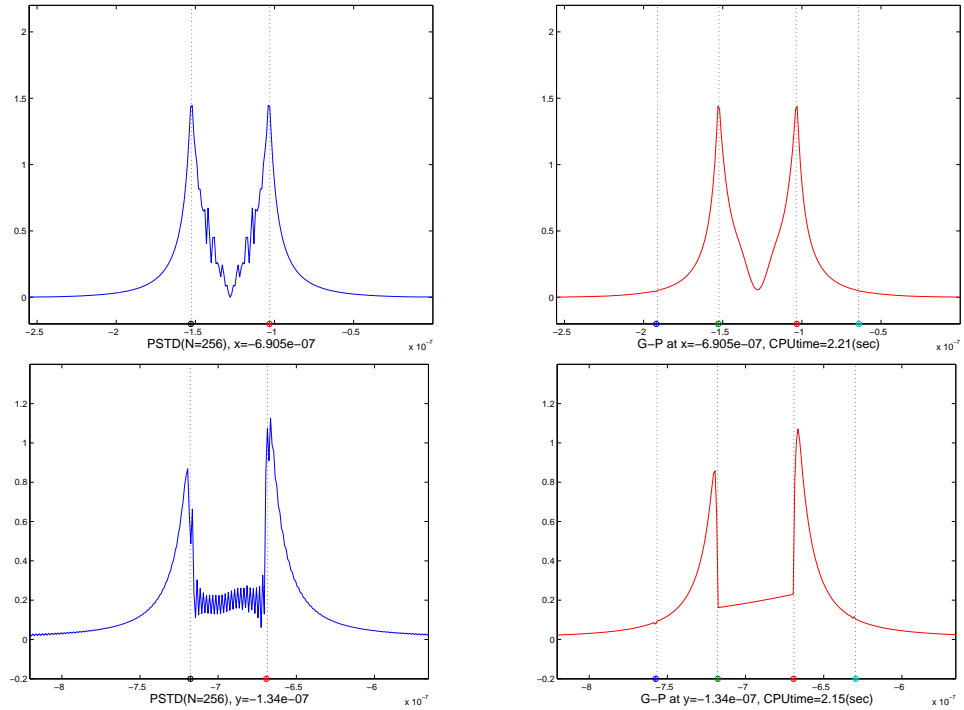


Figure 12: One-dimensional slices for the frequency-domain field distribution of $|E_x|$. Dotted lines indicate the interfaces of the cylinder for the spectral (PSTD: left column) solution and the interfaces of subdomains for the Gegenbauer postprocessed (G-P: right column) solution. Parameters for G-P are chosen as $m = 3, 16, 10, 20, 3$ for five subdomains from left to right with a fixed $\alpha = 1$ (upper right), and similarly $m = 10, 16, 2, 16, 10$ and $\alpha = 4$ (lower right).

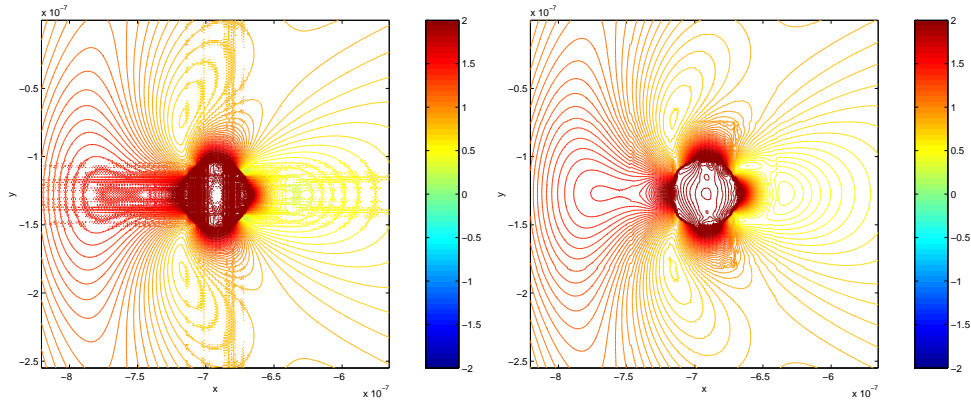


Figure 13: Frequency-domain field distribution of $|E_y|$. From the left: PSTD solution (CPU time= 7893.9 sec on a Mac G5) and its Gegenbauer reconstruction (CPU time = 163.77 sec on an AMD Athlon of 1 GHz).

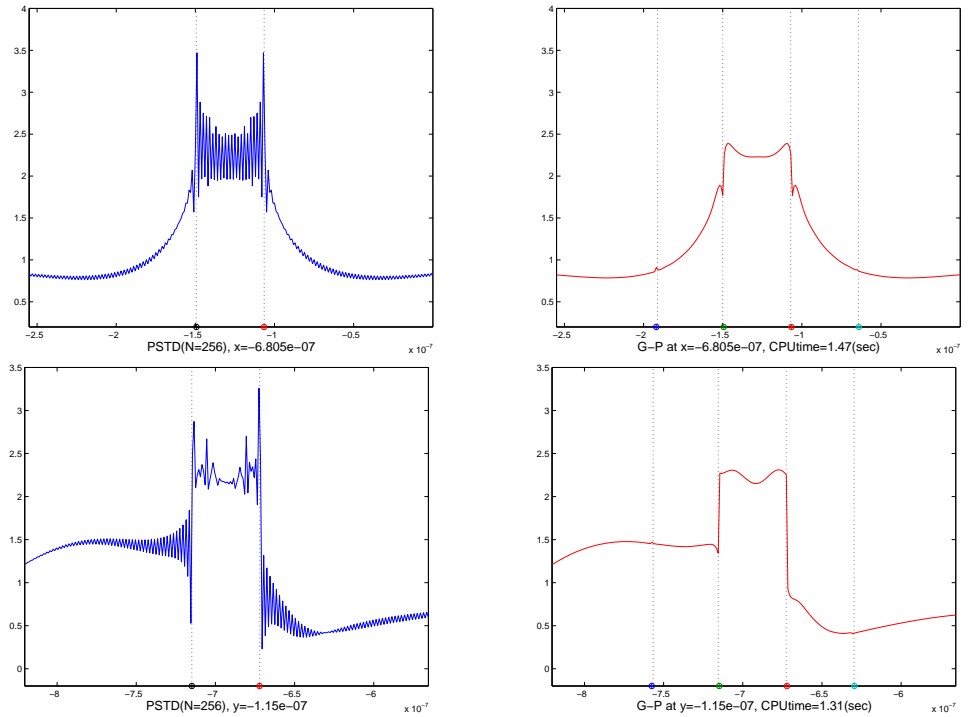


Figure 14: One-dimensional slices for the frequency-domain field distribution of $|E_y|$. Dotted lines indicate the interfaces of the cylinder for the spectral (PSTD: left column) solution and the interfaces of subdomains for the Gegenbauer postprocessed (G-P: right column) solution. Parameters for G-P are chosen as $m = 3, 9, 6, 9, 3$ for five subdomains from left to right with a fixed $\alpha = 3$ (upper right), and similarly $m = 3, 9, 10, 9, 3$ and $\alpha = 2$ (lower right).

6 Conclusion

We have presented a cost-effective Gegenbauer reconstruction technique with a priori knowledge of the location of discontinuities. In one dimension, exponential convergences of the Gegenbauer reconstructions were demonstrated for a nonperiodic and some discontinuous functions. We have extended the implementation to two dimensions and applied it to Fourier-pseudospectral simulations for electromagnetic waves interaction with a nanoscale structure. Successful reductions of the oscillations in Fourier-pseudospectral solutions are obtained after the Gegenbauer reconstructions. Appropriate choices for the parameters were briefly discussed, remaining possible further development for an parameter-free implementation algorithm as future work.

7 Acknowledgements

This work was supported in part by the Mathematics, Information, and Computational Science Division subprogram of the Office of Advanced Scientific Computing Research, Office of Science, U.S. Department of Energy, under contract W-31-109-ENG-38.

References

- [1] M. ABRAMOWITZ, I. A. STEGUN, *Handbook of mathematical functions*, Dover Publications, Inc., New York, 1970.
- [2] W. L. BARNES, A. DEREUX, AND T. W. EBBENSEN, Surface plasmon subwavelength optics, *Nature* 424, pp. 824–830, 2003.
- [3] H. BATEMAN, *Higher transcendental functions*, Vol. 2. McGraw-Hill, New York, 1953.
- [4] CRAIG F. BOHREN, *Absorption and scattering of light by small particles*, John Wiley & Sons, Inc., New York, 1998.
- [5] M. O. DEVILLE, P. F. FISCHER, E. H. MUND, *High-order methods for incompressible fluid flow*, Cambridge University Press, Cambridge, UK, 2002.
- [6] D. FUNARO, *Polynomial approximation of differential equations*, Springer-Verlag, New York, 1991.
- [7] J. D. JOANNOPOULOUS, R. D. MEADE, J. N. WINN, *Photonic crystals: Molding the flow of light*, Princeton University Press, Princeton, NJ, 1995.
- [8] T. LU, P. ZHANG, W. CAI, *Discontinuous Galerkin methods for dispersive and lossy Maxwell's equations and PML boundary conditions*, preprint, 2003.
- [9] Q. H. LIU, *Large-scale simulations of electromagnetic and acoustic measurements using the pseudo-spectral time-domain (PSTD) algorithm*, *IEEE Trans. Geosci. Remote Sensing*, 37, pp. 917–926, 1999.
- [10] C. MIAS, J. P. WEBB, R. L. FERRARI, *Finite element modelling of electromagnetic waves in doubly and triply periodic structures*, *IEE Proc. Optoelectron*, 146, no. 2, pp. 111–118, 1999.
- [11] J. GIBBS, *Fourier's series*, letter in *Nature*, 59, p. 200, 1898.
- [12] D. GOTTLIEB, M. Y. HUSSAINI, S. ORSZAG, *Theory and applications of spectral methods*, in *Spectral methods for partial differential equations*, edited by R. G. Voigt, D. Gottlieb, and M. Y. Hussaini, SIAM, Philadelphia, 1984.
- [13] D. GOTTLIEB, S. ORSZAG, *Numerical analysis of spectral methods: theory and applications*, CBMS-NSF Regional Conference Series in Applied Mathematics, SIAM, Philadelphia, 1977.

- [14] D. GOTTLIEB, C. W. SHU, *On the Gibbs phenomenon IV: Recovering exponential accuracy in a sub-interval from a Gegenbauer partial sum of a piecewise analytic function*, Mathematics of Computation, 64, pp. 1081–1095, 1995.
- [15] D. GOTTLIEB, C. W. SHU, *On the Gibbs phenomenon and its resolution*, SIAM Review, 30, pp. 644–668, 1997.
- [16] S. K. GRAY, T. KUPKA *Propagation of light in metallic nanowire arrays: Finite-difference time domain studies of silver cylinders*, Physical Review B, 68, pp. 045415/1–045415/11, 2003.
- [17] J. M. OLIVA, S. K. GRAY *Theoretical study of dielectrically coated metallic nanowires*, Chemical Physics Letters, 379, pp. 325–331, 2003.
- [18] J. S. HESTHAVEN, D. GOTTLIEB, *Spectral approximation of partial differential equations: Numerical analysis and applications*, Lecture Notes, Brown University, 1996.
- [19] T. W. LEE, S. C. HAGNESS *Pseudo-spectral time domain methods for modeling optical wave propagation in second order nonlinear materials*, Optical Society of America, 2004.
- [20] T. W. LEE, S. C. HAGNESS *A compact wave source condition for the pseudospectral time-domain method*, IEEE Trans. Antennas Propag., 2004 (accepted).
- [21] S. A. MAIER, P. G. KIK, H. A. ATWATER, S. MELTZER, E. HAREL, B. E. KOWEL, A. A. G. REQUICHA, *Local detection of electromagnetic energy transport below the diffraction limit in metal nanoparticle plasmon waveguides*, Nature Materials 2, pp. 229–232, 2003.
- [22] M. S. MIN, *Spectral method for discontinuous problems*, Ph.D. thesis, Brown University, 2002.
- [23] M. S. MIN, D. GOTTLIEB, *On the convergence of the Fourier approximation for eigenvalues and eigenfunctions of discontinuous problems*, SIAM J Numer Anal; 40, no. 6, pp. 2254–2269, 2003
- [24] M. S. MIN, S. M. KABER, W. S. DON, *Fourier-Padé approximations and filtering for the spectral simulations of incompressible Boussinesq convection problem*, Math. Comp., 2004 (accepted).
- [25] Z. S. SACKS, D. M. KINGSLAND, R. LEE, J. F. LEE *A perfectly matched anisotropic absorber for use as an absorbing boundary condition*, IEEE Trans. Antennas Propag., 43, no. 12, pp. 1460–1463, 1995.
- [26] A. TAFLOVE, S. C. HAGNESS, *Computational electrodynamics, the finite difference time domain method*, Artech House, Norwood, MA, 2000.
- [27] K. S. YEE, *Numerical solution of initial boundary value problems involving Maxwell’s equations in isotropic media*, IEEE Trans. Antennas Propag., AP-14, pp. 302–307, 1966.
- [28] R. W. ZIOLKOWSKI, *Time-derivative Lorentz material model-based absorbing boundary condition*, IEEE Trans. Antennas Propag., 45, no. 10, pp. 1530–1535, 1997.

The submitted manuscript has been created by the University of Chicago as Operator of Argonne National Laboratory (“Argonne”) under Contract No. W-31-109-ENG-38. The U.S. Government retains for itself, and others acting on its behalf, a paid-up, nonexclusive, irrevocable worldwide license in said article to reproduce, prepare derivative works, distribute copies to the public, and perform publicly and display publicly, by or on behalf of the Government.